Journal of Chromatography, 648 (1993) 79–90
Elsevier Science Publishers B.V., Amsterdam

CHROM. 25 359

Optimization of pressure-flow limits, strength, intraparticle transport and dynamic capacity by hydrogel solids content and bead size in cellulose immunosorbents

Jeffrey A. Kaster

Department of Chemical Engineering, Virginia Polytechnic Institute and State University, 133 Randolph Hall, Blacksburg, VA 24061 (USA)

Willer de Oliveira and Wolfgang G. Glasser

Department of Wood Science and Forest Products, Virginia Polytechnic Institute and State University, 133 Randolph Hall, Blacksburg, VA 24061 (USA)

William H. Velander*

Department of Chemical Engineering, Virginia Polytechnic Institute and State University, 133 Randolph Hall, Blacksburg, VA 24061 (USA)

(First received October 23rd, 1992; revised manuscript received April 15th, 1993)

ABSTRACT

The design of existing beaded adsorbent materials for column-mode protein purification has emphasized the impact of diffusional transport phenomena upon adsorbent capacity. A design model is presented here that optimizes molecular accessibility of proteins relative to the mechanical stability at low operating pressures by manipulation of size and solids content for uncross-linked cellulose beads. Cellulose beads of several different sizes ranging from about 250 to 1000 μm diameter and having different solids contents were evaluated. Solids content of greater than about 9% cellulose greatly reduced the permeability of large proteins such as thyroglobulin and β-amylase into the beaded matrix at bead contacting times of about 5 and 50 s. Furthermore, the amount of permeation at 3% solids content by thyroglobulin at bead contacting times of about 5 s was about tenfold larger than predicted by diffusion models using the binary diffusivity in a purely aqueous continuum. The utility of a low solids content, large bead cellulose support was shown with immobilized IgG (M_r 155 kDa) capturing recombinant human Protein C (M_r 62 kDa). A 1000 μm diameter beaded cellulose immunosorbent having 3% solids content gave equivalent capacity to a 140 μm diameter beaded, cross-linked agarose support containing 4% solids. In contrast to the smaller diameter, cross-linked beaded agarose, the low solids content beaded cellulose benefitted from greater physical stability due to more optimal pressure-flow characteristics imparted by large bead size.

INTRODUCTION

The chromatographic behavior of packed columns of rigid particles has been well detailed. However, these studies have tended to emphasize the high-pressure liquid chromatography (HPLC) family of very small particles (10 to 50 μm diameter) and have not been well extended to softer hydrogel supports composed of cellulose or agarose derivatives. Soft hydrogel sup-

* Corresponding author.

0021-9673/93/$06.00

ports have been most successfully applied to the immunopurification of large molecules like human plasma proteins such as Protein C (M_r 62 kDa) [1]. The utility of immunosorbents for large scale purifications and the effects of the immobilization chemistry upon antigen binding activity are discussed elsewhere [2]. We discuss here the material aspects of beaded cellulose hydrogels that affect the design of immunosorbents so as to maintain dynamic capacity at high flow rates while generating minimal pressure drop across a column.

The mechanical stability of currently available beaded hydrogels supports is limited at the pressure drops created by high fluid velocities [3]. Immunosorbents commonly consist of cross-linked agarose, cellulose, or synthetic polymer hydrogels with a bead diameter of about 60 to 200 μm and solids contents of less than about 9% (w/w) [4]. Many small agarose or cellulose beaded supports begin to deform at about 4 kPa/cm bed or less followed by an exponential increase in the pressure drop across the column [5]. Furthermore, the velocity at which small bead hydrogel supports crush is inversely proportional to the column diameter [6]. Thus, the strength of hydrogel supports cannot be simply scaled for industrial affinity purification of proteins by increasing the column diameter while holding the bed depth constant [7]. At low fluid velocities, these hydrogels behave roughly as predicted by classical chromatographic theory that has been applied to more rigid HPLC-type supports [8,9].

The processing rates of most chromatographic supports are also limited by the fluid contacting time over which intraparticle diffusional transport can occur. Past hydrogel designs have prioritized a minimization of the path length through which the protein of interest must diffuse in order to be adsorbed. Diffusional transport is particularly slow for proteins, as most have binary diffusion coefficients in water on the order of 10^{-7} cm^2/s or less [10]. The binary diffusion coefficient for proteins in hydrogel support materials would necessarily decrease as the solids content of the hydrogel is increased and diffusional transport becomes hindered.

While the path length for diffusional transport is shortened by decreasing particle size, viscous form drag increases due to an increase in the surface area exposed to flow per volume of support. Therefore, the pressure drop at a given fluid velocity is increased as particle size is decreased. This effect has been well correlated for flow in packed beds of rigid spheres using "Darcy's Law" type expressions such as the Ergun correlation [11]. Thus, the diametrically opposed phenomena of bead penetration and viscous form drag require an optimization of dynamic adsorbent capacity *vs.* throughput at pressure drops that can be supported by the adsorbent and ancillary column equipment. We present here a design model for hydrogel-based immunosorbents that seeks to optimize intraparticle protein transport, physical strength, pressure-flow characteristics, and dynamic capacity by manipulation of bead size and solids content in the particle. Immunosorbents made from cellulose beads are used to evaluate the model and some comparisons to commercially available cross-linked agaroses are made.

EXPERIMENTAL

Cellulose chromatographic supports

Cellulose beads (VPI beads) were produced by regeneration of pure cellulose (Whatman) having a degree of polymerization of about 180–200 [12]. The cellulose was dissolved in a chaotropic, saturated solution of LiCl (9%, w/w) in dimethyl acetamide (DMAC) and the residual insolubles were removed by filtration [13]. Dissolved cellulose concentrations of 0.5–3.3% (w/w) were used. Typically, a batch size of about 0.1–1 l of beads was made by atomization of the cellulose solution into twice the volume of an azeotropic mixture of isopropanol and water or 90% by volume aqueous methanol. A 20 gauge needle was used as an atomizing nozzle. An air jet placed at the tip of the atomizing nozzle was used to disrupt the bead as it emerged from the atomizer. Bead size was varied by adjusting the air jet and cellulose solution flow rate. A single needle could produce up to one l of beads per hour. Extraction of the chaotropic LiCl–DMAC solvent by the aqueous alcohol was achieved by incubation for several hours at room tempera-

ture. This resulted in the regeneration or precipitation of the cellulose as a beaded hydrogel. The beads were then washed in a column mode with 10 bed volumes of water. The solids content of the water-washed cellulose beads was determined by weight loss upon freeze drying of beads that were lightly blotted to remove excess water. Bead size was measured by photomicroscopy of random samples of 15–20 beads. Cellulose beads with diameters less than 250 μm and solids contents ranging from 6 to 13% were kindly provided by SCHZ Lovosice.

Pressure drop

The pressure drop across a column of beaded support was measured at various flow rates. Beads were packed as an aqueous slurry into a 15×1.0 cm column (C10–20, Pharmacia). Degassed deionized water was pumped through the column at various flow rates using a Rainin HPX HPLC pump with a 2070 kPa back-pressure valve in line before the column to maintain pressure on the pump. A KM 5007 I.S. digital pressure gauge (Kane-May) was attached by a three-way valve above the column. The column was first consolidated for a minimum of 30 min at a flow rate that gave a pressure drop of at least 3.4 kPa across the column. The flow rate was then increased incrementally with a minimum of 5 min allowed for the pressure drop across the column to come to equilibrium. The pressure drop was assumed to be asymptotically stable when the change in pressure was less than 0.34 kPa/min. We have defined pressure exponentiation as a greater than 250 kPa change in pressure drop across the column at a set flow rate after exhibiting a stable pressure profile (less than 0.34 kPa change per min) at the previous flow rate.

Permeation studies

Solute permeation in underivatized cellulose beads was studied by elution behavior of single component solutions of dextran, several large proteins and tryptophan (Sigma) relative to that obtained for 0.269 μm latex beads. The elution profiles as detected at 280 nm were studied at two bead contacting times. The chromatographies were run using degassed deionized water for the latex beads and degassed Tris-buffered saline solution (pH 7.0) for the proteins. The permeation studies were run using two flow rates: 0.1 ml/min (0.127 cm/min) and 1.0 ml/min (1.27 cm/min). The void volume of the column was determined using Nanosphere 0.269 ± 0.007 μm polystyrene latex microspheres (Duke Scientific) diluted 1:10 with deionized water.

Cellulose bead activation

Cellulose beads were activated with CNBr by a modification of the method of Porath *et al.* [14]. The beads were blotted to remove excess water, weighed, and 5.0 g were placed in a 40-ml beaker with 5 ml of cold 5 *M* potassium phosphate buffer. The beads and buffer were stirred for 10 min while kept at 0–5°C in an ice bath. CNBr solution (2 ml of 0.1 g/ml CNBr in deionized water) was then added dropwise over 2 min with continuous gentle stirring. The reaction was allowed to continue for an additional 8 min with constant stirring. The reaction was stopped by decanting the beads into a filter and washing with 1 l of 0.1 *M* $NaHCO_3$. Beads were immediately transferred to a 20-ml sample bottle (Wheaton polyethylene scintillation vial, Cole-Parmer) for antibody immobilization.

Immunoglobulin immobilization to CNBr activated beads

A murine anti-human protein C monoclonal antibody, 7D7B10-Mab (American Red Cross), was bound to cellulose or agarose beads by placing 5 mg of 7D7B10-Mab in 2.5 ml coupling buffer (0.1 *M* $NaHCO_3$–0.5 *M* NaCl, pH 8.3) with 5.0 g (preactivated weight) of CNBr activated beads in a 20-ml sample bottle. The immobilization reaction was run overnight at 0–4°C using a turntable agitator. The beads were then washed with two 5-ml deionized water washes to remove free immunoglobulin and unreacted active sites were blocked with 10% ethanolamine in 1 *M* $NaHCO_3$ pH 8.3 for a minimum of 4 h at 0–4°C. The immobilization step was terminated with three alternating washes in 0.05 *M* Na acetate–0.5 *M* NaCl, pH 4.0 and 0.05 *M* Tris–0.5 *M* NaCl, pH 8.0. Beads were stored in TBS pH 7.0 at 0–4°C. The

amount of antibody immobilized was determined by ELISA using the method in refs. 2 and 15.

Column configuration

7D7B10-Mab cellulose or agarose immunosorbent beads (5 ml) were packed into a C10–20 jacketed column (Pharmacia) cooled to 2–6°C with a recirculating cold water bath. Two Rainin HPX pump modules with 100 ml/min pump heads were used for buffer delivery. A 2070 kPa pressure regulator was placed in line upstream of the column to maintain back pressure on the pumps. Protein C-rich feeds were pumped through a Masterflex pump (Cole-Parmer) with a 7013 head for low flow rates (2.5 and 5.0 ml/min) and a 7016 head for high flow rates (10, 20, 40, and 80 ml/min). The pumps and column were connected with low pressure fittings including a three-way valve for preventing back flow into the feed line. Protein content of the column effluent was measured by absorbance at 280 nm with a Knauer Variable Wavelength Monitor UV detector and by ELISA of effluent fractions. A 0.4 mm path length preparative flow cell was used for the 2.5 and 5.0 ml/min runs and a high flow rate variable path length flow cell (Sonntek) was used for all other runs. Buffer delivery and data collection was controlled through Rainin's Dynamax system using a Macintosh Plus computer.

Binding and elution of PC

Recombinant Protein C (rhPC) feed stock was prepared by diluting precentrifuged transgenic pig milk whey–50 m*M* EDTA containing 1 g/l rhPC with degassed 0.1 *M* NaCl, 0.05 *M* Tris, 0.025 *M* EDTA, pH 7.0 (TBS 25 m*M* EDTA) in the ratio: one part whey to three parts TBS 25 m*M* EDTA [16]. The diluted whey was centrifuged for 15 min at 3400 *g* and then gravity filtered to remove precipitates. Diluted clarified whey was stored at 0–4°C for up to 12 h before loading onto the column. During each run, the 7D7B10 cellulose or agarose immunosorbent columns were loaded with 200 ml of the diluted transgenic pig milk whey. The metal dependence of Protein C binding to 7D7B10-Mab (binding of Protein C by 7D7B10-Mab occurs only in the absence of calcium ions) was used to facilitate the elution of the protein from the antibody column [17]. The immunosorbent columns were washed with 18 column volumes of TBS 5 m*M* EDTA after the loading of the whey. The Protein C was eluted with TBS 25 m*M* $CaCl_2$ and 5-ml samples were collected from the start of the elution step. The column was regenerated with successive washes of 4 *M* NaCl, 2 *M* NaSCN, and TBS 5 m*M* EDTA.

Protein C assay

Protein C was assayed using sandwich ELISA with 7D7B10 anti PC Mab as the capturing antibody as described in references 2 and 15.

THEORETICAL

The time that a packet of fluid is in contact with any one bead is defined as the bead contacting time. This bead contacting time is calculated from the bead diameter d_b and the superficial velocity v as follows:

$$t_b = \frac{d_b}{v} \tag{1}$$

The bead contacting time is used to estimate the approximate time available for a species to penetrate the bead.

The analytical equations for diffusion into a sphere have been solved [18]. For this work, the solution for the volume average concentration throughout the sphere has been used as a benchmark to determine the extent of diffusion into the bead assuming that all transport within the bead is diffusive. The analytical solution for the volume average concentration in the bead with the boundary conditions that the concentration at $t = 0$ is $c_0 = 0$ and that the concentration at the surface is c_b for all $t > 0$ is given as:

$$c_{av} = c_b - \frac{6c_b}{\pi^2} \sum_{n=1}^{\infty} \frac{1}{n^2} e^{-D_{PW} n^2 \pi^2 t / R^2} \tag{2}$$

The height equivalent to a theoretical plate (HETP) was calculated from peak width measurements by the standard equation using the half height width:

$$\mathrm{HETP} = \frac{L}{5.545\left(\frac{t_R}{w_h}\right)^2} \tag{3}$$

This equation holds for peaks that are relatively Gaussian [19]. The experimental HETPs were compared to estimated values for HETP given by the correlations of Mikes [20] and Johnson and Stevenson [21].

RESULTS

The amount of cellulose in beads made by regeneration into aqueous alcohol was linearly dependent upon the dissolved cellulose concentration in LiCl–DMAC as shown in Fig. 1. At constant dissolved cellulose concentration, the solids content of the beads was essentially independent of bead size for diameters in the ranges of 1.0–1.8 mm and 0.6–0.8 mm. The standard error ranged from 0.05–0.2% and was calculated for a minimum of three measurements of solids content.

Fig. 2a and b presents the pressure drop *vs.* linear velocities obtained by column mode operation in a 15 × 1.0 cm packed bed for VPI beads of the present work and various commercially available beaded agaroses. Fig. 2a gives pressure drop *vs.* linear velocities obtained by column mode operation for VPI beads of different solids content having a size of about 600–700 μm diameter. Pressure exponentiation occurs for beads containing 1% solids at superficial velocities greater than about 15 cm/min (Fig. 2a; curve 1). Pressure exponentiation occurs for beads containing 1.2% solids at superficial velocities of greater than about 40 cm/min (Fig. 2a; curve 2). Pressure exponentiation occurs for beads containing 1.9% solids at superficial velocities of greater than about 70 cm/min (Fig. 2a; curve 3). Beads containing 3.2% solids did not exhibit a

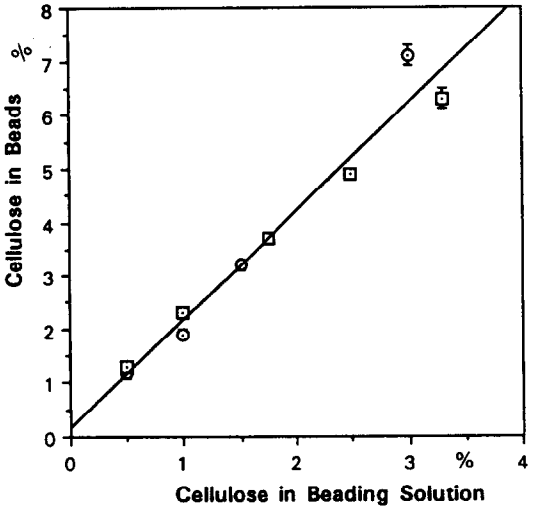

Fig. 1. Mass percent cellulose in beads as a function of solution concentration. □ = Large beads, 1.0–1.8 mm in diameter; ○ = small beads, 0.6–0.8 mm in diameter.

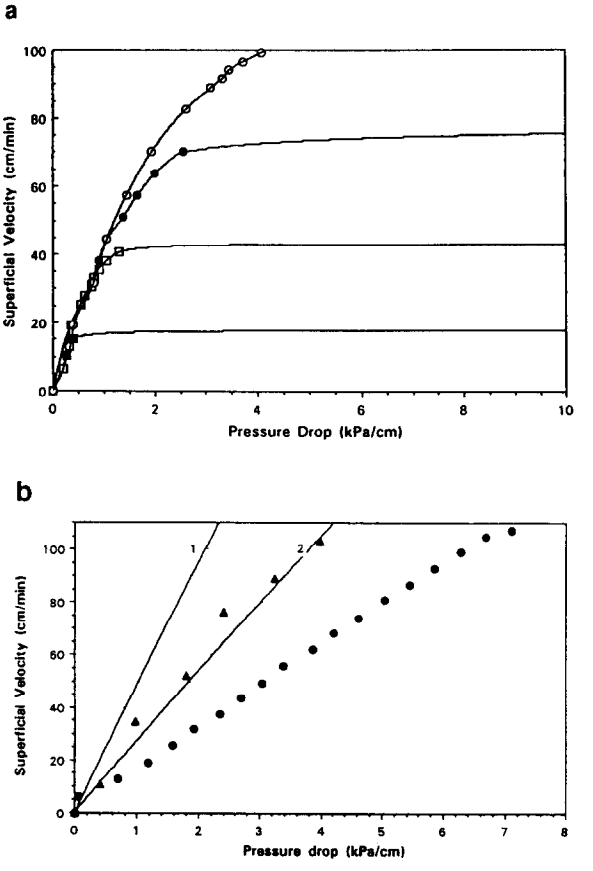

Fig. 2. (a) The effects of solids content on the pressure drop curve. VPI cellulose beads in a 15.0 × 1.0 cm column. (1) ■ = 600 μm diameter beads, 0.9% solids (w/w); (2) □ = 700 μm diameter beads, 1.2% solids; (3) ● = 800 μm diameter beads, 1.9% solids; (4) ○ = 700 μm diameter beads, 3.2% solids. (b) Pressure drops across columns of nominal 300 μm beads. Experimental results plotted in comparison to the theoretical results of the Ergun equation [11]. ● = Sepharose 6MB (250 ± 40 μm diameter cross-linked agarose beads, 9% solids), ▲ = VPI cellulose beads (340 ± 40 μm diameter cellulose beads, 9% solids); (1) theoretical 250 μm diameter beads, (2) theoretical 340 μm diameter beads.

pressure exponentiation at flow rates up to 100 cm/min (Fig. 2a; curve 4).

Fig. 2b compares the observed pressure-flow behavior of uncross-linked 9% cellulose (300–380 μm diameter) and cross-linked 9% agarose (250–300 μm diameter) with the predicted pressure-flow behavior of idealized rigid spheres having diameters of 340 μm (Fig. 2b, curve 1) and 250 μm (Fig. 2b, curve 2). No pressure exponentiation at velocities up to about 100 cm/min was seen for either bead. The Ergun equation [11], a semi-empirical prediction of pressure drop as a function of flow rate for rigid spheres, shows that both cellulose and cross-linked agarose yield more pressure drop than that predicted for rigid spheres of the same size.

Fig. 3 plots the crushing velocity, percent solids content and bead size from the above data for VPI beads and Perloza cellulose beads (SCHZ Lovosice). We term the crushing velocity as the superficial velocity (ml flow/min/cm^2 bed area or cm/min) at which the pressure drop across the column exponentiates. Low crushing velocities (about 5–10 cm/min in a 15 cm column) are seen in beads with solids content less than about 6% (w/w) and with size smaller than about 200 μm in diameter.

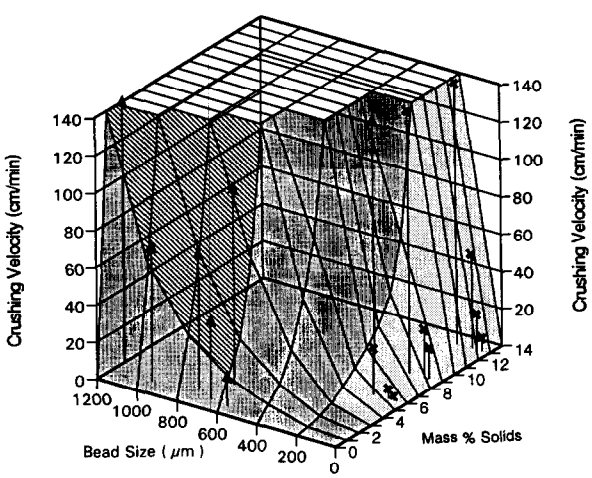

Fig. 3. Relationship between bead size, composition, and crushing velocity. × = Cellulose beads of less than 200 μm, courtesy of SCHZ Lovosice; ▲ = cellulose beads of present work. Dark shaded area = projected crushing velocity as a function of bead size and weight percent solids; hatched area = approximate projected surface defining the performance and composition of VPI beads; lightly shaded area = approximate projected surface defining the performance and composition of commercially available beads.

Fig. 4A, B, C, and D presents permeation chromatography done on underivatized cellulose beads ($\approx$1000 μm) at superficial velocities of 0.12 cm/min ($t_b \approx 50$ s) and 1.2 cm/min ($t_b \approx 5$ s). Cellulose beads with solids contents of 3%, 4%, 6%, and 9% with average diameters of about 1000 μm were studied. As indicated by a sharp elution peak of 0.269 μm diameter latex polymer spheres, void volumes ranged from 0.40–0.45 column volumes for all beads analyzed (Fig. 4A, B, C, and D; panel a). The void volumes did not vary with linear velocity. For any of the biochemical species evaluated in these permeation experiments; after about 1.5 column volumes, no absorbance was detected in the subsequent 10 column volumes.

Permeation experiments using blue dextran (M_r 2 000 kDa) in 3% cellulose beads gave an elution profile at 0.12 cm/min having two maxima with about 80% of the O.D. 280 nm centered at about 0.5 column volumes with the remainder being more broadly centered at about 1.0 column volumes (Fig. 4A; panel b). The elution profile for blue dextran at 1.2 cm/min gave a single maximum at about 0.5 column volumes (Fig. 4B; panel b). Thyroglobulin (M_r 669 kDa) also gave a bimodal elution pattern, but greater than 80% of the protein was centered about 1.0 column volumes with the remainder centered at about 0.45 column volumes for the 0.12 cm/min trial (Fig. 4A; panel c). A shift to about 50% of the absorbance at 280 nm centered at about 0.5 column volumes occurred at a superficial velocity of 1.2 cm/min for thyroglobulin. β-amylase (M_r 200 kDa) gave a broad elution peak with a maximum at 1.0 column volumes at 0.12 cm/min which shifted to about 0.75 column volumes at 1.2 cm/min. Tryptophan gave an elution peak centered about 1.0 column volumes at both velocities with a slight peak broadening occurring at 1.2 cm/min. Permeation experiments using cellulose beads of 4.8% and 6% solids content showed similar results with full penetration of small and intermediate species but excluding the blue dextran (data not shown).

Permeation experiments of blue dextran,

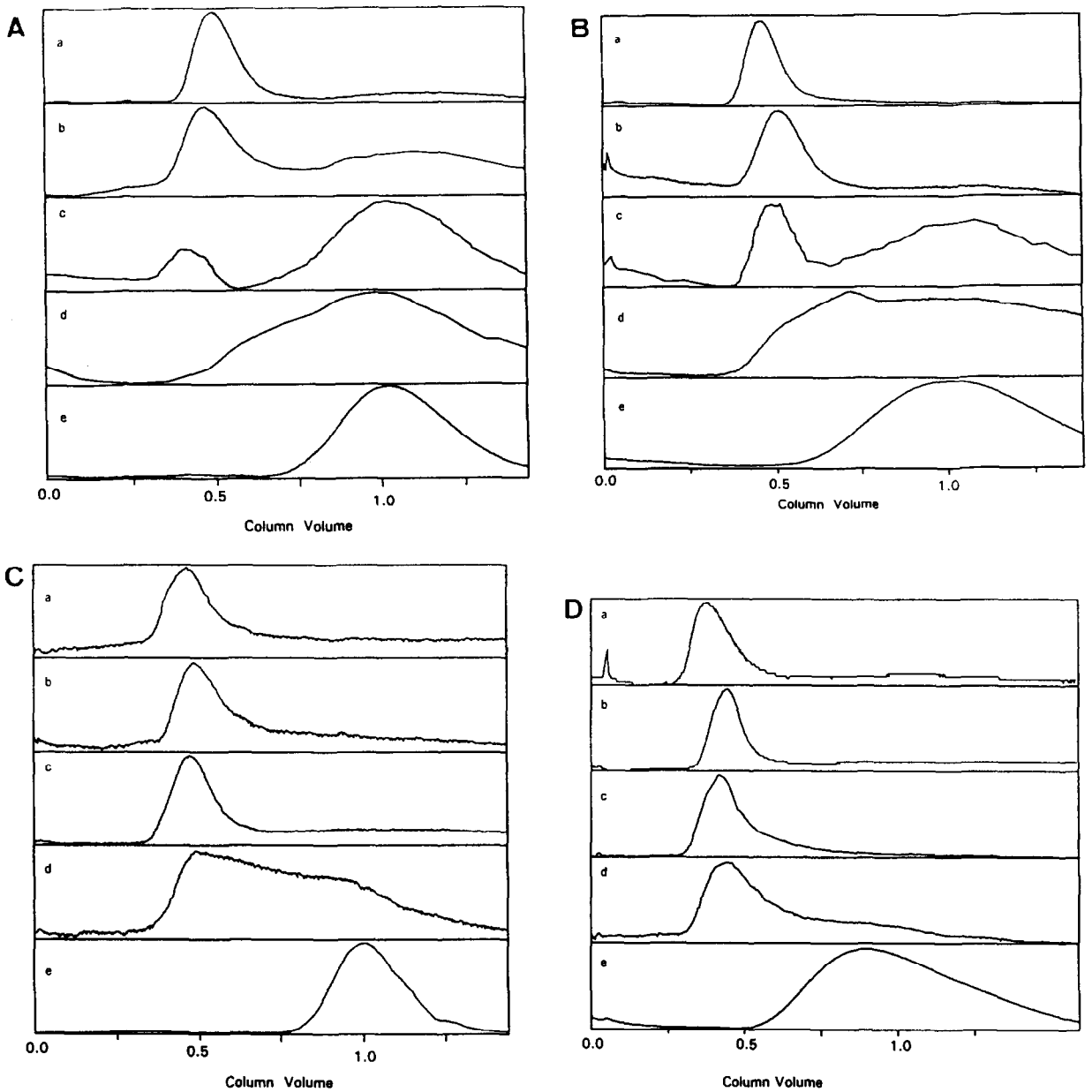

Fig. 4. Gel permeation chromatography on 3% (1 mm) cellulose beads (A, B) and 9% (0.8 mm) cellulose beads (C,D). Column: 35.4 × 1.0 cm. (A) superficial velocity, 0.12 cm/min, bead contacting time, 47 s. (B) Superficial velocity, 1.2 cm/min, bead contacting time, 5 s. (C) Superficial velocity, 0.12 cm/min, bead contacting time, 40 s. (D) Superficial velocity, 1.2 cm/min, bead contacting time, 4 s. a = Nanosphere 0.269 μm microspheres; b = blue dextran, molecular mass 2 000 000; c = thyroglobulin, molecular mass 669 000; d = β-amylase, molecular mass 200 000; e = tryptophan, molecular mass 204.

thyroglobulin, and β-amylase in 9% cellulose beads gave similar elution profiles at both 0.12 cm/min and 1.2 cm/min (Fig. 4C and 4D; panels b, c and d, respectively). The elution profile for the above large molecular mass species gave a single maximum at about 0.5–0.6 column vol-

TABLE I

RESIDENCE TIMES IN IMMUNOAFFINITY EXPERIMENTS

Support material	Bound antibody	Superficial velocity (cm/min)	Column residence time (s)	Bead contacting time [a] (s)	Eluted antigen binding efficiency (%)
3% Cellulose beads[b]	7D7B10	3.2	124	1.9	17 ± 5
		6.4	62	1.0	17 ± 3
		12.7	31	0.5	13 ± 2
		25.5	16	0.2	12 ± 1
		50.9	8	0.1	8 ± 1
		101.9	4	0.06	3 ± 3
4% Cross-linked agarose beads[c]	7D7B10	3.2	106	0.3	19 ± 1

[a] Bead contacting time calculated as column residence time × the ratio of the bead size to the column length.
[b] ≈ 1000 μm diameter beads.
[c] ≈ 140 μm diameter beads.

umes. In contrast, tryptophan gave an elution peak centered about 1.0 column volumes at both velocities with a slight peak broadening occurring at 1.2 cm/min (Fig. 4C and 4D; panel e).

The results of immunoaffinity adsorption experiments using cross-linked agarose and uncross-linked cellulose beads in a column loading and elution mode are listed in Table I. The column loading of the target protein was done at the same superficial velocity as the elution of product in each set of experiments. Both supports contained approximately 1 mg of immobilized Mab per ml hydrogel. Column residence and bead contacting times are given in Table I for each set of experiments. At column residence times of about 60 s or greater ($t_b \geq 1$ s), the amount of Protein C captured and eluted by the immobilized monoclonal antibody on 3% cellulose beads (≈ 1000 μm in diameter) was similar to that measured for the same antibody immobilized on the cross-linked 4% agarose beads (≈ 140 μm in diameter) column ($t_b = 0.3$ s). The capacity of the cellulose and agarose immunosorbents decreased significantly at t_b of about 0.5 s or less.

DISCUSSION

Fig. 5a combines the gross exclusion criteria of cellulose beads reported in the literature (with solids content greater than about 6%) with data obtained here for the VPI beads. We have here defined exclusion as greater than 80% of peak area at O.D. 280 nm appearing in the void volume at a linear velocity of about 1.2 cm/min or less (the void volume being taken as 0.40–0.45 column volumes). The data from Fig. 5a suggests the design criteria shown in Fig. 5b for the production of useful beaded cellulose sorption materials for protein purification. We have applied these criteria to the design of immunosorbents for the efficient capture of human Protein C (M_r 62 kDa) by an IgG class Mab (M_r 155 kDa). Larger proteins like thyroglobulin (M_r 669 kDa) and β-amylase (M_r 200 kDa) were also shown to permeate beads having 3% solids content.

The transport phenomena affected by changes in particle size and solids content are opposing in their impact upon chromatographic throughput and adsorbent capacity. Thus, when taken together, the data presented above suggest an optimization process illustrated in Fig. 5b. A "window of acceptable support characteristics" for a soft hydrogel is defined by the opposing effects of molecular accessibility, mechanical strength in a flow field, and the percentage of solids in the hydrogel. The lower limit for solids content at any given bead size is determined by the mechanical strength of the hydrogel as manifested by crushing velocity at a given bed depth. A minimum solids content of the gel at a given bead size might be chosen such that the crushing velocity is several-fold higher than the desired

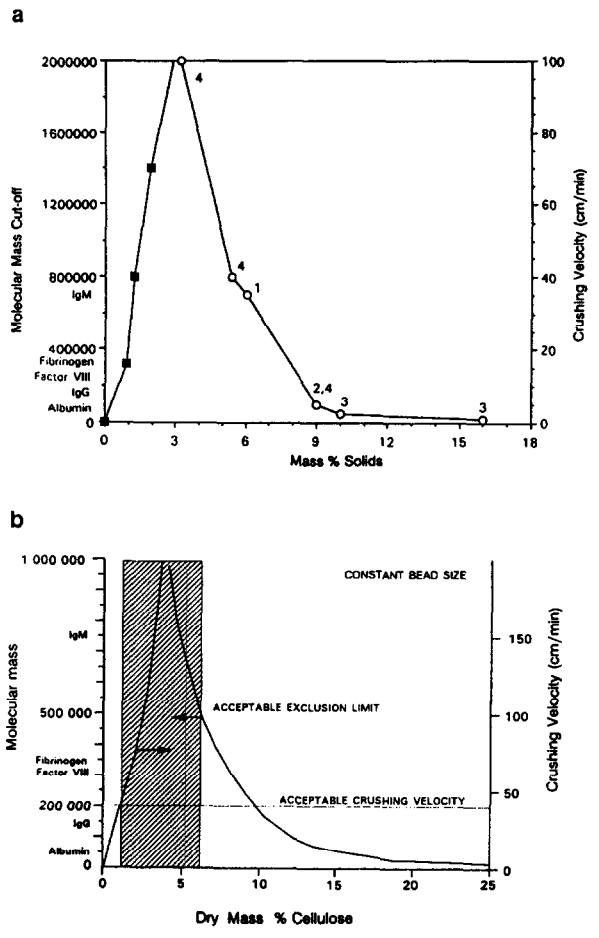

Fig. 5. (a) Data summary of molecular exclusion (greater than 90% excluded) and crushing velocity of various cellulose supports. ■ = Crushing velocity of VPI cellulose beads, ○ = molecular mass exclusion limit of various cellulose beads. 1 = Perloza cellulose beads; 2 = Kuga [23]; 3 = Peska *et al.* [24]; 4 = VPI cellulose beads. (b) Design characteristics for cellulose supports.

maximum operating superficial velocity. Because intraparticle transport is usually rate limiting, an estimate of the bead contacting time (t_b) can be used to determine a suitable operating velocity.

We have included a broad range of bead sizes as an important dimension of support characteristics. Fig. 3 shows the nonlinear relationship between crushing velocity, bead size, and solids content of cellulose hydrogels. It is noted that the least desirable matrices from the consideration of strength under flow are those that combine small bead size and low solids content.

The remaining variable not presented in Fig. 3 is dynamic capacity. Therefore, the 1000 μm diameter beads having 3% solids were evaluated for immunosorptive capacity since they possessed both molecular accessibility and sufficient physical strength under the flows which would exceed that needed for small or large-scale immunopurification processing. At a t_b of about 1 s, large cellulose beads exhibited immunosorptive efficiencies similar to 140 μm diameter agarose beads, as shown in Table I. Efficiency calculations are based upon an assumption of two antigens captured and eluted per immobilized antibody. Relative to the small cross-linked agarose immunosorbent, the cellulose immunosorbent could operate at shorter column residence times since faster flow rates could be sustained without risk of crushing. The fast throughput of the cellulose media occurred at a greatly decreased pressure drop due to increased bead size. Our analysis also included a comparison of cellulose beads of similar size to available agaroses. Because the strength of cellulose beads was similar to that of cross-linked agarose of a similar size and solids content, some of the design rationale developed here for larger cellulose beads may be applicable to the design of large bead agaroses used for immunosorbents. At the same low Mab densities used here, the dynamic capacity of both cellulose and agarose beads may be due to Mab immobilized near the surface. However, the cellulose beads gave similar capacities with eightfold less surface area per volume than the agarose beads. In addition, the peak widths seen in the immunoaffinity experiments were significantly smaller than would be predicted by the diffusion based, semi-empirical correlations of Mikes [20] and Johnson and Stevenson [21]. As shown in Table II, the experimental HETP (eqn. 3) for the cellulose immunosorbent was predicted to be 130 cm for a 1000 μm bead while the actual HETPs measured were about 0.4–0.9 cm. The experimental HETP for agarose beads with equivalent immunosorbent capacity was found to be about that of the cellulose. In the case of the small agarose beads, the HETP calculated by the above correlations agreed well with the experimental values.

We have attempted to grossly characterize the

TABLE II

HEIGHT EQUIVALENT TO A THEORETICAL PLATE: EXPERIMENTAL RESULTS *VS.* THEORY

Beaded material	System	Particle diameter (mm)	Superficial velocity (cm/min)	Experimental HETP[a] (cm)	Calculated HETP Johnson and Stevenson[b] (cm)	Calculated HETP Mikes[c] (cm)
Sepharose CL-4B (Agarose)	Immunoaffinity	0.14	2.5	0.4	0.6	0.7
VPI (Cellulose)	Immunoaffinity	1.2	13	0.4–0.9	132	134
	Gel permeation	1.2	0.13	0.9	0.5	0.5
	Tryptophan		1.3	1.8	2.8	3.2
	Gel permeation	1.2	0.13	1.0	5.2	6.1
	Thyroglobulin		1.3	0.9	49	58

[a] Calculated from eqn. 3.
[b] Ref. 21.
[c] Ref. 20.

transport of large and small molecules into the underivatized cellulose bead containing 91–97% water. The structure of these low solids content cellulose beads is likely stabilized by dispersed regions that have a high degree of hydrogen bonding. Preliminary studies of bead morphology by photomicroscopic evaluation of 10 μm cross-sections infiltrated with polymeric fixative indicate a homogeneous distribution of solids content in underivatized and derivatized cellulose beads (data not shown). In addition, no visible changes in bead appearance such as size or shape occurred as a result of Mab derivatization. We therefore studied the intraparticle transport from permeation experiments on underivatized beads to help understand the transport phenomena in Mab derivatized beads. The cost of Mab in making large columns of immunosorbents prevented us from doing permeation experiments on the immunosorbent columns proper.

The 3–9% range of solids contents studied here was chosen in an attempt to identify a transition of hydrogel structure from a very sparse density of low diffusional resistance to sufficient density to sterically encumber diffusional transport of proteins. We hypothesize that the transition regime for transport of proteins would consist of three experimentally identifiable modes of intraparticle transport phenomena. First, in approaching the limit of an aqueous continuum at very low solids content, a mixture of convective and diffusive modes of intraparticle transport would be expected to occur for even large molecules such as proteins. This would be a transport regime that would be faster than that predicted from diffusion alone. Second, a perturbation to slightly higher solids content would be expected to dampen out intraparticle convection and result in diffusion being the dominant mode of intraparticle transport. This intermediate solids content would not be expected to exert significant steric hindrance to diffusing proteins. Third, at still higher solids content, a transition to significant steric exclusion resulting from a higher density of gel structure would prevent diffusional transport of large proteins into the interior of the bead.

For cases where the solids content is low enough to eliminate the effects of steric exclusion, an estimate of the penetration solely by diffusion can be made by analytical solution [22]. Additional correlations that incorporate the effect of diffusion have been developed to describe chromatographic performance such as elution peak width [20,21]. The discussion below makes comparisons of estimates of intraparticle diffusional transport from both the analytical solution of diffusion into an aqueous sphere and predictions of peak width using chromatographic performance correlations.

The binary diffusion coefficient of tryptophan

TABLE III

EXTENT OF DIFFUSION IN GEL PERMEATION EXPERIMENTS BY THE ANALYTICAL SOLUTION

Species	Molecular mass	$D_{PW} \times 10^6$ cm^2/s	Extent of diffusion ($c_{av}/c_\infty \times 100$)			
			$t = 4$ s, $d_b = 0.8$ mm	$t = 5$ s, $d_b = 1$ mm	$t = 40$ s, $d_b = 0.8$ mm	$t = 50$ s, $d_b = 1$ mm
Tryptophan	204	5.0	34.1	30.9	82.2	77.0
β-Amylase	200 000	0.4	10.4	9.3	30.9	27.9
Thyroglobulin	669 000	0.26	8.4	7.6	25.3	22.9
Blue dextran	2 000 000	0.0583	4.0	3.6	12.5	11.2
Nanospheres 0.269 μm	N.A.	0.0126	1.9	1.7	5.9	5.3

in water is approximately twenty times larger than that of thyroglobulin [10]. Table III provides an estimate of the percentage of the equilibrium volume average concentration (c_{av}/c_b, eqn. 2) that could be achieved in the bead at the various bead contacting times (t_b, eqn. 1) estimated for the permeation data presented here. Permeation of tryptophan should have occurred to about 80% of equilibrium ($c_{av}/c_b = 0.8$) at $t_b = 50$ s and only about 30% of the equilibrium value ($c_{av}/c_b = 0.3$) should have been reached at $t_b = 5$ s. Thus, permeation could have occurred if the diffusion coefficient in the bead were the same as that of a purely aqueous continuum. The experimental HETPs for tryptophan at $v = 0.13$ and 1.3 cm/min were similar to that predicted by the diffusion based HETPs calculated by the methods of Mikes [20] and Johnson and Stevenson [21]. In summary, the gel permeation behavior of tryptophan in particles having 3–9% solids content is well described by diffusional transport in a homogeneous aqueous media.

The degree of permeation by large proteins such as thyroglobulin into 3% beads having 1000 μm average diameter at about 50 or 5 s bead contacting times was significantly more than would have been predicted by a purely diffusive transport. We have estimated that thyroglobulin should have permeated these beads to less than 25% of equilibrium ($c_{av}/c_b = 0.25$) at $t_b = 50$ s or to less than 8% of equilibrium ($c_{av}/c_b = 0.08$) at $t_b = 5$ s (Table III). The experimental HETP from the thyroglobulin permeation in 3% cellulose beads at $t_b = 50$ s was about 1.0 cm while the predicted HETP was about 5–6 cm. Furthermore, the experimental HETP at $t_b = 5$ s was about 0.9 cm as compared to the predicted HETP of 49–58 cm (Table II). Some of the bimodal aspects of the elution profile of thyroglobulin may be due to aggregation or nonspecific adsorption to the cellulose. Beads having 9% solids content appeared to exclude both blue dextran and thyroglobulin at $t_b = 40$ and 4 s. The elution behavior of β-amylase at $t_b = 40$ s was similar for both 3% and 9% cellulose beads. However, β-amylase did not appear to significantly permeate at $t_b = 4$ s in 9% cellulose beads. Thus, the β-amylase permeation behavior in 9% cellulose beads may be indicative of a gel structure that imparts significant hindrance to diffusion of large proteins. The lack of permeation by blue dextran in 9% cellulose beads of this work is similar to those reported by Kuga [23] and Peska *et al.* [24] which used cellulose beads having bead diameters less than about 200 μm. The rapid intraparticle transport of large proteins in the 3% cellulose beads observed in these studies may be evidence of an intraparticle transport regime having both convection and diffusion.

CONCLUSIONS

Using the above design rationale, we have developed large bead cellulose immunoaffinity sorbents which have equivalent capacity and

immunosorbent efficiency (utilization of coupled antibody) to that of smaller beaded hydrogel immunosorbents. It appears that beads of 3% solids content show some characteristics of enhanced intraparticle mass transfer over that explainable by unhindered diffusion. We are currently elucidating the dynamic immunosorbent capacity of beaded cellulose hydrogels derivatized with higher loadings of Mab to determine the extent of penetration of the immobilized IgG into the cellulose beads.

ACKNOWLEDGEMENTS

We thank professors L. Wang, S. Cramer and C.F. Ivory for their valuable comments. Special thanks to K. Van Cott for his help and comments in the editing process. This work was partially funded by National Science Foundation Grants BCS-9011098 and CBT-8803036 to W.H.V.

SYMBOLS

c_0	initial concentration of protein in bead (mg ml^{-1})
c_b	bulk fluid protein concentration (mg ml^{-1})
c_{av}	volume average concentration of protein in bead (mg ml^{-1})
CV	dimensionless throughput "column volume" ($= vt / L$)
d_b	diameter of bead (cm)
D_{PW}	diffusion coefficient of the protein through water ($cm^2\ s^{-1}$)
HETP	height equivalent to a theoretical plate (cm)
L	length of the column (cm)
M_r	molecular mass (kDa)
R	radius of bead (cm)
t	time (s)
t_b	bead contacting time ($= d_b/v$) (s)
t_R	retention time of a protein in the column (s)
v	superficial velocity of the bulk fluid through the column (cm s^{-1})
w_h	peak width measured at half the height of the peak (s)

REFERENCES

1 W.H. Velander, T. Morcol, D.B. Clark, D. Gee and W.N. Drohan, *Adv. Appl. Biotechnol.*, 11 (1990) 11–27.
2 C.L. Orthner, F.A. Highsmith, J. Tharakan, R.D. Madurawe, T. Morcol and W.H. Velander, *J. Chromatogr.*, 558 (1991) 55–70.
3 S.L. Fowell and H.A. Chase, *J. Biotechnol.*, 4 (1986) 1–13.
4 K. Kang, D. Ryu, W.N. Drohan and C.L. Orthner, *Biotechnol. Bioeng.*, 39 (1992) 1086–1092.
5 L.F. Chen and G.T. Tsao, *Biotechnol. Bioeng.*, 18 (1976) 1507–1516.
6 S. Katoh, *Trends Biotechnol.*, 5 (1987) 328–331.
7 Y.D. Clonis, *Bio/Technology*, 5 (1987) 1290–1293.
8 F.H. Arnold, W.H. Blanch and C.R. Wilke, *Chem. Eng. J.*, 30 (1985) B9–B23.
9 F.H. Arnold, W.H. Blanch and C.R. Wilke, *Chem. Eng. J.*, 30 (1985) B25–B36.
10 M.T. Tyn and T.W. Gusek, *Biotechnol. Bioeng.*, 35 (1990) 327–338.
11 R.E. Treybal, *Mass-Transfer Operations*, McGraw-Hill, 3rd ed., 1980, p. 200.
12 W.H. Velander, J.A. Kaster and W.G. Glasser, *US Pat. Appl.*, 07/496 314.
13 C.L. McCormick and D.K. Lichatowich, *J. Polym. Sci., Polym. Lett. Ed.*, 17 (1979) 479–484.
14 J. Porath, K. Aspberg, H. Drevin and R. Axen, *J. Chromatogr.*, 86 (1986) 53–56.
15 W.H. Velander, A. Subramanian, R. Madurawe and C.L. Orthner, *Biotechnol. Bioeng.*, 39 (1992) 1013–1023.
16 W.H. Velander, A. Subramanian, A.W. Degener, T. Morcol, J.L. Johnson, T.D. Wilkins, F.C. Gwazdauskas, R.M. Akers, H. Lubon and W.N. Drohan, *ACS Proceedings of the Meeting: Harnessing Biotechnology for the 21st Century*, 1992.
17 W.H. Velander, R.D. Madurawe, C.L. Orthner, J.P. Tharakan, A.H. Ralston, D.K. Strickland and W.N. Drohan, *Biotechnol. Prog.*, 5(3) (1989) 119–125.
18 H.S. Carslaw and J.C. Jaeger, *Conduction of Heat in Solids*, Oxford University Press, Oxford, 2nd ed., 1978, pp. 233–237.
19 R.W. Yost, L.S. Ettre and R.D. Conlon, *Practical Liquid Chromatography: An Introduction*, Perkin Elmer, 1980, pp. 38–41.
20 O. Mikes in Z. Deyl, K. Macek and J. Janak (Editors), *Liquid Column Chromatography: A Survey of Modern Techniques and Applications*, Elsevier, 1975, pp. 82–83.
21 E.L. Johnson and R. Stevenson, *Basic Liquid Chromatography*, Varian, Palo Alto, CA, 1978, pp. 15–31.
22 J.R. Welty, C.E. Wicks, R.E. Wilson, *Fundamentals of Momentum, Heat, and Mass Transfer*, John Wiley and Sons, New York, 2nd ed., 1976, pp. 561–569, 711–725.
23 S. Kuga, *J. Chromatogr.*, 195 (1980) 221–230.
24 J. Peska, J. Stamberg, J. Hradil and M. Ilavsky, *J. Chromatogr.*, 125 (1976) 455–469.